Application of artificial neural network models and random forest algorithm for estimation of fracture intensity from petrophysical data

Marzieh Zaiery[1] · Ali Kadkhodaie[2] · Mehran Arian[1] · Zahra Maleki[1]

Abstract

Natural fractures play an essential role in the characterization and modeling of hydrocarbon reservoirs. Modeling fractured reservoirs requires an understanding of fracture characteristics. Fractured zones can be detected by using seismic data, petrophysical logs, well tests, drilling mud loss history and core description. In this study, the feed-forward neural networks (FFNN), cascade feed forward neural networks (CFFN) and random forests (RF) were used to determine fracture density from petrophysical logs. The model performance was assessed using statistical measures including the root mean squared error (RMSE), coefficient of determination (R^2), mean absolute error (MAE), Kling Gupta efficiency (KGE) and Willmott's index (WI). Conventional good logs and full-bore micro-resistivity imaging data were available from three drilled wells of the Mozduran reservoir, Khangiran gas field. According to the findings of this research, the FFNN model showed a higher KGE and WI, and a higher correlation coefficient (R^2) compared to the CFNN model. The CFNN model outperformed the FFNN model with lower neurons. The models' performance was also improved by increasing the number of neurons in the hidden layers from 8 to 35. The findings of this study demonstrate that the measured and FFNN calculated fracture intensity is in excellent agreement with image log results showing a correlation coefficient of 92%. The RF algorithm showed higher stability and robustness in predicting fracture intensity with a correlation coefficient of 93%. The results of this study can successfully be used as an aid in a more successful reservoir dynamic modeling and production data analysis.

Keywords Fracture density · Petrophysical image logs · Random forest model · Production data · Artificial neural network

Abbreviations

ANFIS	Adaptive neuro-fuzzy inference system
ANN	Artificial neural network
CFFN	Cascade feed forward neural network
CFN	Continuous fracture network
DNF	Discrete fracture network
DT	Sonic log
FFNN	Feed-forward neural network
FMI	Formation micro imager
GR	Gamma ray log
NPHI	Neutron porosity log
OOB	Out of bag
PEF	Lithology
PHIE	Effective porosity
PHIT	Porosity
RF	Random forest
RHOB	Density
R^2	Coefficient of determination
VOL_CALCIT	Volume of calcite
VOL_DOLOM	Volume of dolomite

List of symbols

Ij	Relative importance of jth variable
KGE	Kling Gupta efficiency
MAE	Mean absolute error
N	Number of data points
N_h	Number of hidden neurons
N_i	Number of input variables
R	Regression coefficient
RMSE	Root mean squares error
W	Connection weight
WI	Willmott's index
X mi	Observed value
X m	Mean observed value

✉ Mehran Arian
  mehranarian@yahoo.com

1 Department of Earth Sciences, Faculty of Converging Sciences and Technologies, Science and Research Branch, Islamic Azad University, Tehran, Iran

2 Earth Sciences Department, Faculty of Natural Sciences, University of Tabriz, Tabriz, Iran

| X pi | Predicted value |
| α (SDR) | Standard deviation ratio |

Introduction

Natural fractures are the most significant factors determining the hydraulic behavior of oil and gas reservoirs. Proper knowledge of fractures is essential in oil production and development plans. In general, fractures play a significant part in the production of fractured reservoirs (Kadkhodaie et al. 2021; Derafshi et al. 2022; Pejic et al. 2022; Hosseinzadeh et al. 2023). Natural fractures in reservoirs range from large to small-scale fractures. Large-scale fractures are like significant faults seen at seismic sections. Different methods have been proposed to identify small-scale fractures around the well (e.g. Kosari et al. 2015, 2017; Pejic et al. 2022; Mazdarani et al. 2023). One of the methods is to use petrophysical logs such as neutron, density and sonic. However, they are not accurate enough due to their low resolution. This method is cost-effective and is currently in use. Image logs of the formation; provide essential information about fractures, such as their dip and azimuth, fracture spacing, fracture density and aperture. In addition, by interpreting them, other geological features such as stratification, stylolite, faults and anhydrite nodes can be identified. Image logs can identify fractures in the excellent way with a high resolution. Using image logs in a well is economically expensive and is acquired in a few wells of a hydrocarbon field. In this study, an artificial intelligence approach was used to derive image log-derived fracture parameters from petrophysical logs quickly with reliable accuracy. Numerous studies on the characterization of naturally fractured reservoirs have been conducted recently. Tokhmechi et al. (2010) utilized the power of petrophysical logs and a novel technique for estimating fracture density in fractured zones. In their study, the energy of the petrophysical logs was calculated in the fractured zones and linear and nonlinear regressions were established between them. Their investigation demonstrated a significant relationship between fracture density and the energy of calipers, sonic (DT), density (RHOB) and lithology (PEF) logs in each well. Using artificial neural networks and conventional well logs calibrated to core data, Zazoun (2013) implemented a model that can forecast fracture density (ANNs). Ja'fari et al. (2011) presented a model that uses an adaptive neuro-fuzzy inference system to estimate fracture density using conventional good logs. Their results demonstrated that the observed and neuro-fuzzy calculated fracture density may be reconciled well (correlation coefficient of 98%). Aghli et al. (2019) proposed employing the preprocessed petrophysical logs as a trustworthy and affordable tool to assess the fracture parameters in the heterogeneous carbonate reservoir based on Adaptive Neuro-Fuzzy

Inference System (ANFIS) technique. The results show that conventional well logs might be improved as instrumental tools for evaluating fractures if they were statistically preprocessed and coupled with image logs or core data. They found a high correlation between petrophysical logs and images or cores results ($R^2 = 0.8$). Zerrouki et al. (2014) used four conventional log data consisting of deep resistivity, density, neutron porosity and gamma-ray to predict fracture porosity using fuzzy ranking and artificial neural network (ANN).

In this paper, a new method is presented for estimating fracture intensity using a combination of image logs, petrophysical logs, and artificial intelligence networks.

Geological setting

The Khangiran gas field is an NW–SE structure located in the northeastern part of Khorasan Razavi province, near the political border with Turkmenistan, around 180 km northeast of Mashhad city in Iran (Fig. 1). This field is situated in the Kopet Dagh Basin, and its neighboring field in Iran is Gonbadli Field and Dauletabad Field in Turkmenistan. The Kopet-Dagh Basin is located southern margin of the Amu-Darya basin which is a highly productive petroleum province in Turkmenistan and Uzbekistan, extending southwestward into Iran and southeastward into Afghanistan. The Hercynian accreted terrane made up of deformed and commonly metamorphosed Paleozoic rocks forms the basement of the Amu-Darya Basin. The Upper Jurassic carbonates (Mozduran Formation) and Lower Cretaceous sandstones (Shurijeh Formation) are the two reservoir sequences hosting giant


Fig. 1 Location map of Khangiran gas field, northeastern, Iran

gas reserves in Khangiran Field. The Relationship between sedimentary basins (e.g., Khavari et al. 2009, Arian et al. 2012, Arian and Aran 2014, Ehsani and Arian 2015, Aram and Arian 2016) and basement faulting (e.g., Arian (2012), Nouri et al. (2013a, b), Nouri and Arian (2017), Nabilou et al. (2018) and Mansouri et al. (2017, 2018) indicates the role of faults in controlling the sedimentary basins of NE Iran. In terms of lithofacies, especially the role of tectonics in the sedimentary basins, Arian (2015), Razaghian et al.

(2018) and Taesiri et al. (2020) divided sedimentary basins of Iran into several large scale tectonic-stratigraphic zones. In the study area, a northwest-southeast rift has been formed at early Jurassic. The rift developed as a back-arc basin for the Neotethyan Ocean and the Mozduran and Shurijeh Formations were deposited, but the deformation of the basin started from Eocene by inversion tectonics. The stratigraphic chart of Kopet-Dagh Basin is shown in Fig. 2. To data a total of 77 wells have been drilled in the Khangiran Field (22

Fig. 2 Stratigraphic column of Kopet-Dagh Basin, modified from Robert et al. (2014)
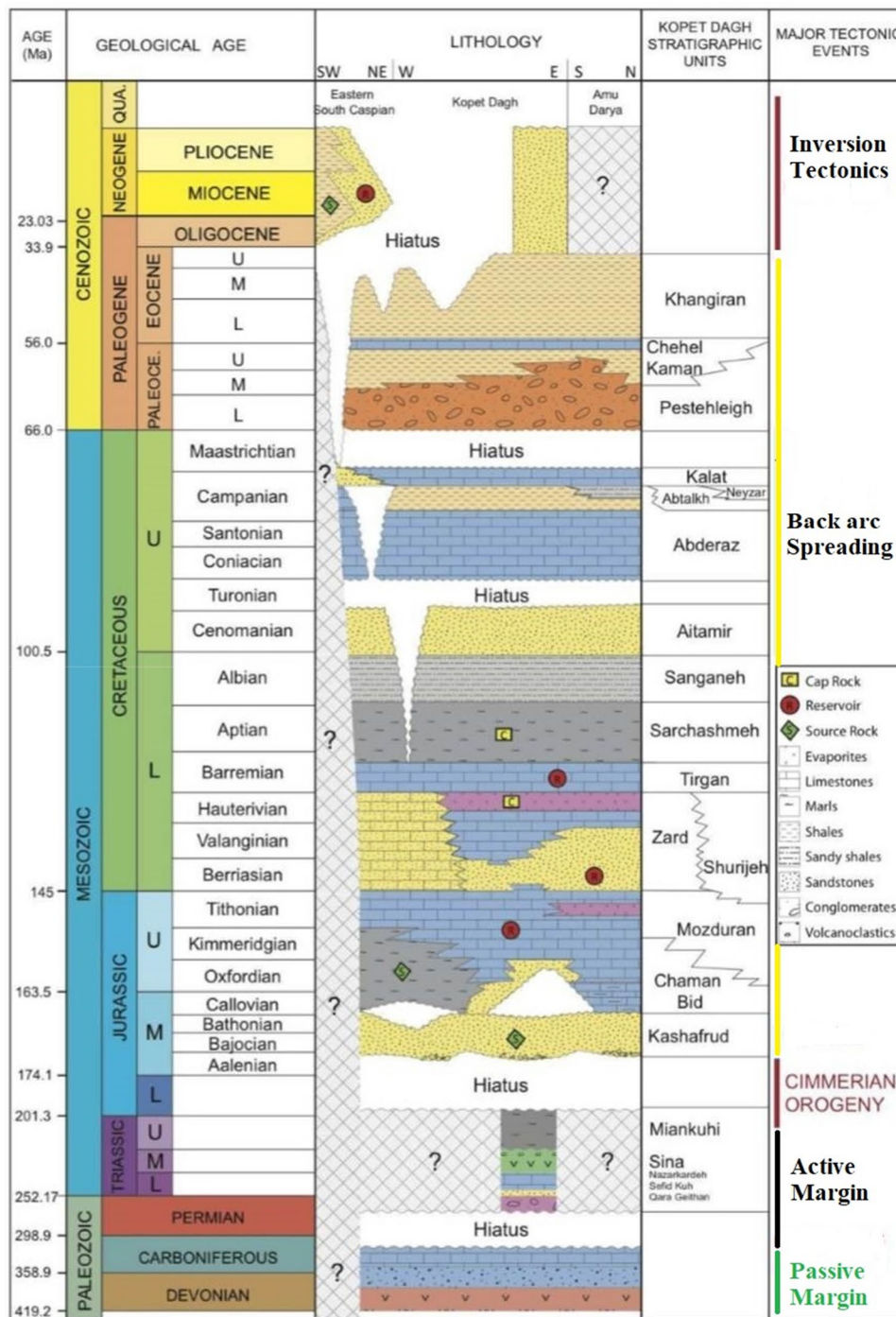
wells in Shurijeh Formation, 51 wells in Mozduran Formation, three wells in the Kashafrud formation, and one well is under drilling during the preparing of this manuscript. It should be noted that the number of wells, which were completed in the Shurijeh, Mozduran and Shurijeh-Mozduran formations are 31, 40, and 2, respectively. Most of the carbonate rocks of the Mozduran formation were deposited in a carbonate platform adjacent to a deeper marine environment. The slope and basial environment were separated from an extensive shelf lagoon and tidal flat by platform margin ooid/bioclast grain stones forming a rimmed shelf platform. The vertical sequence of the Mozduran formation indicates five significant episodes of deepening and shallowing (Callovian to early Kimmeridgian), with numerous shallowing-upward Para sequences. Both tectonic and Autocycles mechanisms are suggested as the main cause of the generation of these cycles.

Materials and methods

Data collection

The dataset used in this study was taken from an oil field in northeastern Iran. To date, a total of 77 wells had been drilled in the field, and of which has both image logs and petrophysical logs data. The fracture densities were derived from image logs interpretation, and after a resampling process, the correlation between well logs and fracture intensity was investigated. The relationship between the fracture intensity and well log data, including Depth (Depth), sonic log (DT), gamma ray log (GR), volume of dolomite (VOL_DOLOM), volume of calcite (VOL_CALCIT), porosity (PHIT), effective porosity (PHIE), neutron porosity log (NPHI) and bulk density log (RHOB) is summarized in Table 1. A total of 70% of the data were used as the training dataset, and the remaining 30% were utilized as the testing and validation dataset. Identical inputs were exposed to the models in both training and testing phases to compare the accuracy of the models.

It should be noted that the training dataset were not used to test the model's performance. To estimate the fracture zones and their densities, the current study used FFNN and CFFNN methodologies. The network architectures of FFNN and CFFNN are comparable. An input layer, one or more hidden layers and an output layer are all features of the structures. Signal transmission between neurons differs between the two systems; FFNN only transmits neurons from the input layer to the output layer, but CFFNN is not confined to one-way transfers, and each layer is connected with both preceding and succeeding levels (Warsito et al. 2018). Cascade Forward Neural Network (CFNN) is a kind of artificial neural network (ANNs) that is extensively used for

Table 1 Statistical indexes of the petrophysical input logs and fracture intensity

Statistical parameters	DEPTH (m)	DT ($\mu s/ft$)	GR (API)	NPHI (fr)	RHOB (gr/cm³)	PHIE (fr)	PHIT (fr)	VOL_CALCITE (fr)	VOL_DOLOM (fr)	Fracture Intensity (m^{-1})
Min	3046.93	44.40	1.77	0.00	2.09	0.00	0.00	0.00	0.00	0.00
Max	3504.59	68.16	133.69	0.19	2.87	0.17	0.17	0.98	1.00	12.56
Mean	3226.92	53.61	8.05	0.05	2.66	0.04	0.04	0.19	0.74	1.74
Std. deviation	132.68	4.25	10.85	0.03	0.11	0.04	0.04	0.34	0.34	2.13

predicting numerous applications (Ac and Avc 2016; Badde et al. 2012; Elbita et al. 2014; Ganesh et al. 2018; Zhao et al. 2020; Gündodu and Elbir 2021). Any input-to-output mapping may also utilize it. While CFNN and FFNN are similar, CFNN has links between each layer's inputs and previous layers. Each neuron in the input node of a CFNN is linked to another neuron in the hidden and output nodes, which is the only difference between them (Karaca 2016).

Artificial neural networks (ANNs)

In recent decades, artificial neural networks (ANNs) have become a prominent AI method. They have been used in various fields, including geosciences and engineering. An artificial neural network (ANN) is a computer tool that can link factors influencing a complicated event. It is inspired by the human brain and comprises many essential processing components (Raikar 2004). The ANN model is trained using a collection of input data, then it can make predictions. In general, an ANN operation starts with data processing in neurons (nodes) and signals are exchanged between nodes through connections. Each connection has a weight assigned to it depending on the relevance of the nodes it connects. To identify the output signal from the input signal, each node employs a nonlinear activation function (Raikar 2004). Most multilayer ANNs have three layers: an input layer, one or more hidden layers and an output layer, with each layer containing many neurons. ANN technologies have been presented in a variety of ways, and they are classified in a variety of ways. Feedforward (perceptron) networks, competitive networks and recurrent networks are the three main types of

ANNs employed for prediction problems in earth sciences (Vaghefi et al. 2020).

Model development

FFNN and CFFNN As previously mentioned, the FFNN and CFFNN algorithms use many neurons as input and output variables in the input and output layers. A network for the fracture properties was necessary for the current investigation. As illustrated in Figs. 3 and 4, a network with nine neurons in the input layer and one in the output layer was utilized to estimate fracture intensity based on the gathered data.

The number of hidden layers, the number of neurons in each hidden layer, the activation function and the training process all affect the models accuracy (Vaghefi et al. 2020). There is no reliable method for determining these values. As a result, they are estimated by trial and error (Mahmoodi et al. 2018). Earlier research has shown that the Levenberg–Marquardt algorithm is one of the most efficient and acceptable training algorithms compared to the other standard training methods (Huang et al. 2006). As a result, the Levenberg–Marquardt training method was used in this study for fracture intensity estimation. In addition, the hidden layer used a sigmoid transfer function, whereas the output layer used a linear transfer function. According to Bishop (1995), no more than two hidden layers are usually required. Using trial and error, the current work increased the number of hidden layers from 1 to 5, with 1–40 neurons in each layer. Two hidden layers were found to have the maximum accuracy. It was also discovered that the model's accuracy changed with each iteration for a certain number of hidden layers and neurons. This has been reported

Fig. 3 Feed-forward neural network architecture for fracture intensity estimation
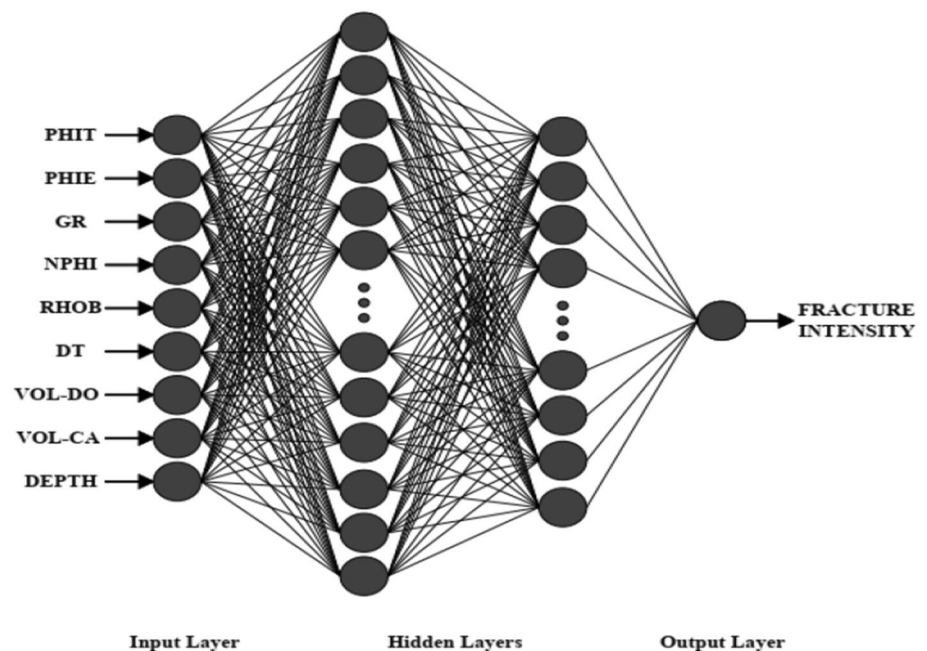
Fig. 4 Cascade feed forward neural network for fracture intensity estimation
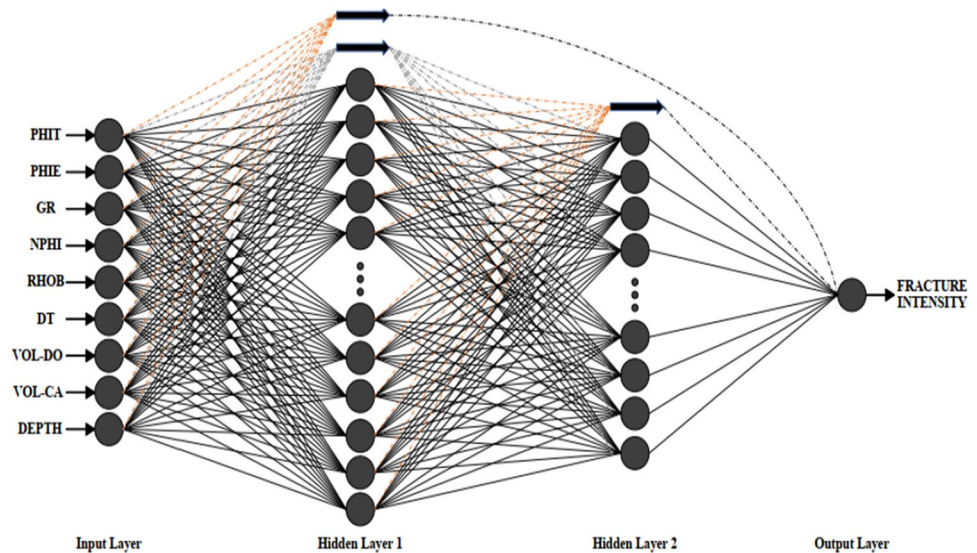
in previous publications (Vaghefi et al. 2020). To get the best accuracy, the model was iterated 50 times for each variation in the number of hidden layers and neurons.

Evaluation of the models

To assess the model's efficacy and accuracy, the correlation coefficient (R), Kling Gupta efficiency (KGE), Root Mean Square Error (RMSE), Mean Absolute Error (MAE) and Willmott's Index (WI) were utilized as follows:

$$\mathbf{RMSE} = \sqrt{\frac{1}{\mathbf{N}} \sum_{\mathbf{i=1}}^{\mathbf{N}} \left(\mathbf{X_{mi}} - \mathbf{X_{pi}}\right)^2} \tag{1}$$

$$\mathbf{R} = \frac{\sum_{\mathbf{i=1}}^{\mathbf{N}} \left(\mathbf{X_{mi}} - \overline{\mathbf{X}}_\mathbf{m}\right)\left(\mathbf{X_{pi}} - \overline{\mathbf{X}}_\mathbf{p}\right)}{\sqrt{\sum_{\mathbf{i=1}}^{\mathbf{N}} \left(\mathbf{X_{mi}} - \mathbf{X_m}\right)^2 \sum_{\mathbf{i=1}}^{\mathbf{N}} \left(\mathbf{X_{pi}} - \mathbf{X_p}\right)^2}} \tag{2}$$

$$\mathbf{MAE} = \frac{1}{\mathbf{N}} \sum_{\mathbf{i=1}}^{\mathbf{N}} \left|\left(\mathbf{X_{mi}} - \mathbf{X_{pi}}\right)\right| \tag{3}$$

$$\mathbf{KGE} = 1 - \sqrt{(\mathbf{R} - 1)^2 + (\boldsymbol{\alpha} - 1)^2 + (\boldsymbol{\beta} - 1)^2} \tag{4}$$

where X_{mi} is the observed value, X_{pi} is the predicted value, R is the correlation coefficient of observed and predicted values, $\overline{X}_m$ is the mean observed value, α is the standard deviation ratio (SDR) of X_{mi} and X_{pi}, β is the mean ratio of X_{mi} and X_{pi}, and N is the number of data points. The optimal model would be determined by its R, KGE, and WI values, as well as its RMSE and MAE values.

Results and discussion

The performance evaluation of the models

The advantages of cascade neural networks are well known. First, no structure of the networks is predefined; that is, the network is automatically built up from the training data. Second, the cascade network learns fast because each of its neurons is trained independently of the other. However, a disadvantage is that the cascade networks can be over-fitting in the presence of noisy features. To overcome this problem, we used the random forest algorithm. A random forest is a collection of Decision Trees; each, Tree independently makes a prediction and the values are then averaged (Regression)/Max voted (Classification) to arrive at the final value. The accuracy of Random Forest is generally very high; its efficiency is particularly Notable in large datasets, and provides an estimate of essential variables in classification; Forests Generated can be saved and reused, unlike other models, it does not overfit with more features.

Table 2 compares the accuracy of the ANN models in estimating fracture intensity. As can be observed, each model performed well and was accurate in the fracture intensity estimation derived from the image logs data. The FFNN had the lowest estimation error, while the CFFNN had the greatest, according to the indices used in the testing step. During the testing phase, the RMSE for the estimation of the fracture intensity for FFNN-7 was 0.395 1/m. The RMSE of the FFNN-7 model was lower than that of the CFFNN by 43.54, 54.71 and 64.94 percent.

Furthermore, in fracture intensity estimation, FFNN showed a KGE of 0.975 in the testing step, being as high as 2.67%, 13.02%, and 15.89% greater than CFFNN. This suggests that FFNN outperformed CFFNN. Figure 5

Table 2 The accuracy of the ANN models in estimating the fracture intensity from petrophysical data

| ANNs architecture		RMSE		MAE		KGE		WI		R²	Best linear fitting
		Train	Test	Train		Train	Test	Train	Test	All	
FFNN-1	9-08-08-1	2.31	1.14	2.54	1.15	0.62	0.64	0.61	0.44	0.70	$y = 0.48x + 1.3$
CFFNN-1	9-08-08-1	1.03	2.15	0.76	0.97	0.63	0.63	0.62	0.56	0.86	$y = 0.77x + 0.56$
FFNN-2	9-12-09-1	0.91	0.70	1.82	0.96	0.76	0.78	0.72	0.76	0.86	$y = 0.78x + 0.52$
CFFNN-2	9-12-09-1	0.88	1.35	0.69	0.95	0.72	0.74	0.68	0.72	0.85	$y = 0.82x + 0.43$
FFNN-3	9-15-10-1	0.89	0.69	1.64	0.89	0.80	0.81	0.86	0.82	0.89	$y = 0.85x + 0.39$
CFFNN-3	9-15-10-1	0.88	1.21	0.63	0.93	0.76	0.78	0.81	0.78	0.89	$y = 0.82x + 0.45$
FFNN-4	9-20-11-1	0.71	0.61	1.58	0.89	0.88	0.89	0.88	0.86	0.87	$y = 0.76x + 0.53$
CFFNN-4	9-20-11-1	0.84	0.68	1.73	0.89	0.84	0.85	0.84	0.82	0.87	$y = 0.78x + 0.51$
FFNN-5	9-25-12-1	0.62	0.58	1.57	0.85	0.90	0.90	0.90	0.90	0.91	$y = 0.87x + 0.35$
CFFNN-5	9-25-12-1	0.77	0.67	1.79	0.83	0.86	0.87	0.85	0.86	0.87	$y = 0.75x + 0.57$
FFNN-6	9-30-15-1	0.43	0.47	1.51	0.85	0.94	0.91	0.93	0.93	0.89	$y = 0.83x + 0.31$
CFFNN-6	9-30-15-1	0.77	0.64	1.44	0.79	0.90	0.88	0.89	0.89	0.87	$y = 0.78x + 0.56$
FFNN-7	9-35-20-1	0.40	0.45	1.49	0.82	0.99	0.98	0.98	0.95	0.93	$y = 0.89x + 0.27$
CFFNN-7	9-35-20-1	0.65	0.58	1.08	0.75	0.95	0.94	0.94	0.91	0.91	$y = 0.83x + 0.42$
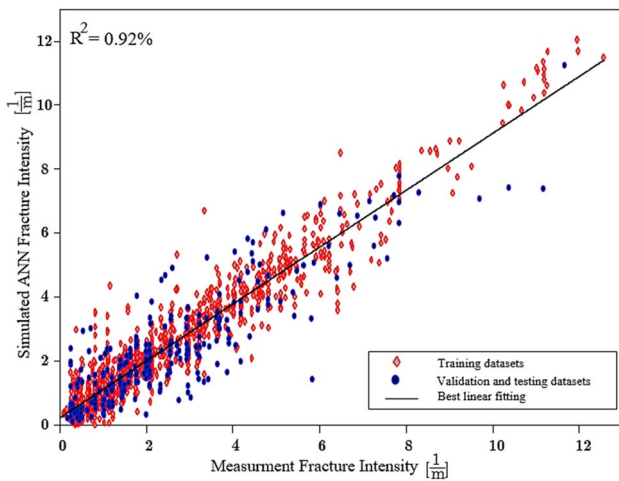
Fig. 5 The FFNN-predicted intensity of fracture profiles for one of the test wells (FFNN-7). As is seen, the FFNN-predicted profiles are in good agreement with the image log observations

represents the scatter plots for the observed versus modeled data for the fracture intensity estimation. As is seen, the models with a correlation coefficient greater than 0.9 could explain the measurements with reasonable accuracy. FFNN shows the highest correlation of $R = 0.995$ in fracture intensity estimation. A comparison of measured and estimated fracture intensity using FFNN is shown in Fig. 6.

Fracture intensity model based on RF algorithm

A popular tree-based machine-learning methodology is the Random Forest (RF) method (Breiman 2001; Mohana et al. 2021). Random Forest, in addressing complex correlations
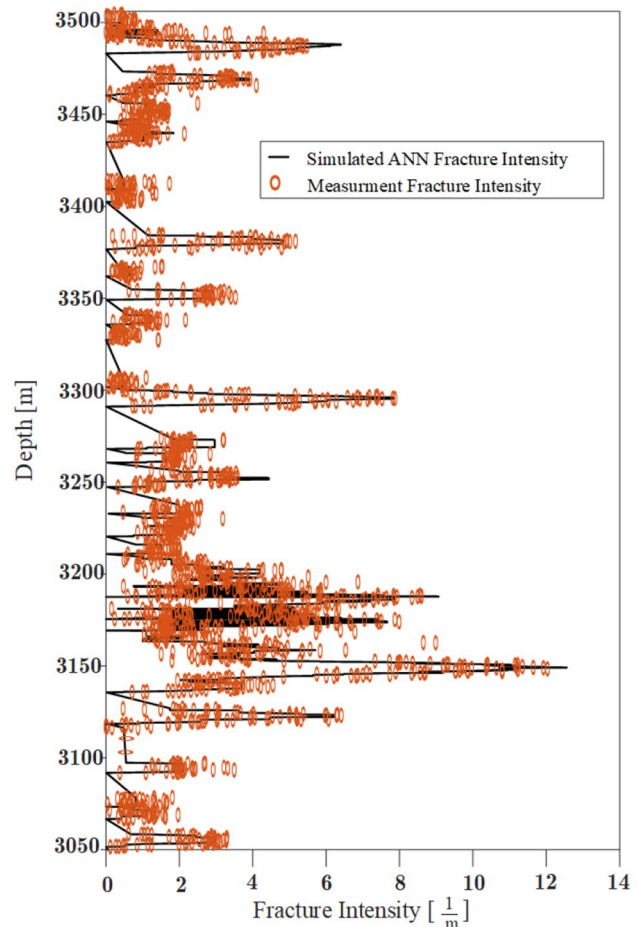
Fig. 6 A comparison of measured and estimated fracture intensity by using FFNN

between variables, has risen in favor in recent years because of its ability to correctly foresee complicated relationships between variables (Matin et al. 2016; Matin and Chelgani 2016). The RF algorithm uses a unique sampling method called bootstrap sampling to increase the diversity of sample selection. The two forms of data created in this technique are out-of-bag (OOB) data and in-bag data. OOB data refers to the 1/3 of the original sample removed from the bag, whereas in-bag data relates to the remaining sample (Lei et al. 2018).

This bootstrap dataset is used to generate many decision trees. Numerous decision trees are created from this bootstrap dataset and combined to get much more accurate and stable prediction. RF does not depend on a single decision tree; instead, it takes predictions from the individual trees and predicts the outcome depending on the majority of votes. Cross-plots showing the correlation coefficient between the measured and estimated fracture density using the random forest algorithm in the training and test dataset are shown in Fig. 7.

Sensitivity analysis (SA)

Garson (1991) devised a method (Eq. 5) based on the weight matrix for the estimation of the relative relevance of each input parameter. The relative influence of each input variable (mentioned in Fig. 8) on fracture intensity is graphically shown in Fig. 8.

$$I_j = \frac{\sum_{m=1}^{m=N_h} \left(\left(\left| W_{j_m}^{i_h} \right| / \sum_{k=1}^{N_i} \left| W_{k_m}^{i_h} \right| \right) \times \left| W_{m_n}^{h_0} \right| \right)}{\sum_{m=1}^{m=N_i} \left\{ \left(\sum_{m=1}^{m=N_h} \left| W_{k_m}^{i_h} \right| / \sum_{k=1}^{N_i} \left| W_{k_m}^{i_h} \right| \right) \times \left| W_{m_n}^{h_0} \right| \right\}} \quad (5)$$
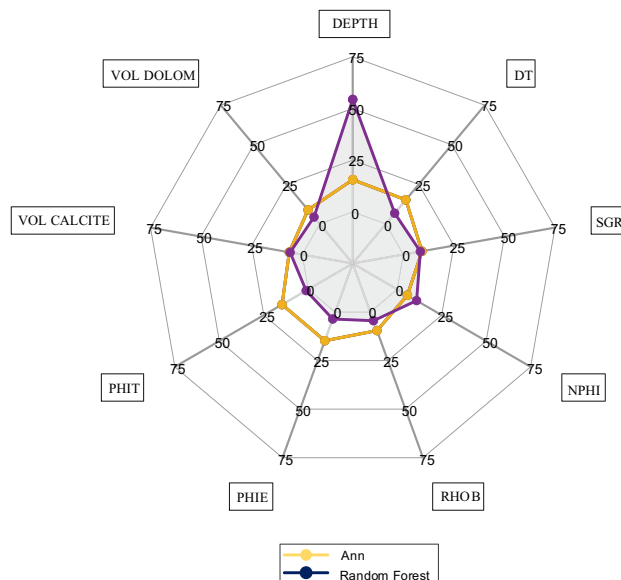
where

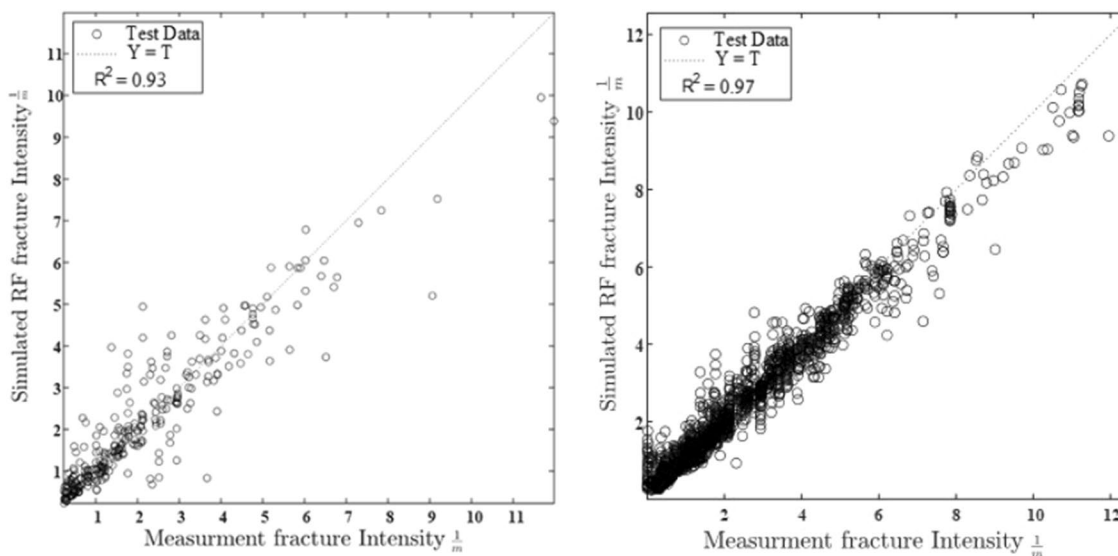I_j = relative importance of jth variable.

N_i = number of input variables.

N_h = number of hidden neurons.

W = connection weight.

Fig. 8 Radar diagrams for influential input variables by the FFNN and random forest models for the Fracture intensity

Fig. 7 Cross plots showing the correlation coefficient between the measured and estimated fracture density using the random forest algorithm in the training and test data set

The letters *i*, *h*, and *o* stand for input, hidden, and output layers, respectively, whereas the letters *k*, *m*, and *n* stand for input, hidden, and output neurons. Figure 8 shows how the FFNN and random forest models compare in identifying the essential inputs. The depth profile in the random forest model may be regarded to be the influencing variable introduced into the model by post-processing procedures.

Conclusions

In the current study, attempts were made to formulate petrophysical data into fracture intensity derived from image logs interpretation. Followings are concluded.

- The Feed-Forward Neural Network (FFNN), the Cascade Feed Forward Neural Network (CFFNN) and the Random Forest (RF) methods were used in the current work to forecast the fracture density using petrophysical log data including depth, gamma ray, neutron, density, effective porosity, total porosity, calcite volume and dolomite volume.
- The models were developed utilizing the results of image logs interpretation. Evaluation of the models showed that FFNN and RF resulted in satisfactory results. There is a good agreement between the measured and estimated fracture intensity. Post-processing techniques were used to evaluate the significance of input variables.
- The results indicated that the FFNN with the lowest error outperformed the CFFNN models in fracture intensity estimation. The comparative study indicates the superior capacity of the random forest to forecast fracture intensity in terms of the correlation coefficient, stability and robustness.
- In the absence of expensive image logs such as full-bore formation micro imager (FMI), using the intelligent models can forecast fracture intensity from easily available well logging data. This will enhance the applicability of well logs for extraction of further parameters in addition to their routine job for petrophysical evaluation of hydrocarbon reservoirs.
- The well log-derived fracture intensity data can be used to construct continuous fracture network (CFN) and discrete fracture network (DNF) models and study the impact of fracture models on production.

Author contribution MZ: Conceptualization, Methodology, Data curation, Software, Writing—original draft. AK: Conceptualization, Supervision, Validation. MA: Conceptualization, Visualization, ZM: Investigation, Writing—review & editing.

Declarations

References

Acı M, Avcı M (2016) Artificial neural network approach for atomic coordinate prediction of carbon nanotubes. Appl Phys A. https://doi.org/10.1007/s00339-016-0153-1

Aghli G, Moussavi-Harami R, Mortazavi S, Mohammadian R (2019) Evaluation of new method for estimation of fracture parameters using conventional petrophysical logs and ANFIS in the carbonate heterogeneous reservoirs. J Petrol Sci Eng 172:1092–1102. https://doi.org/10.1016/j.petrol.2018.09.017

Aram Z, Arian M (2016) Active tectonics of the Gharasu River Basin in Zagros, Iran, investigated by Calculation of geomorphic indices and group decision using analytic hierarchy process (AHP) software. Episodes 39:39–44

Arian M (2012) Clustering of Diapiric Provinces in the Central Iran Basin. Carbonates Evaporites 27:9–18

Arian M (2015) Seismotectonic-geologic hazards zoning of Iran. Earth Sci Res J 19:7–13

Arian M, Aram Z (2014) Relative tectonic activity classification in the Kermanshah Area, Western Iran. Solid Earth 5:1277–1291

Arian M, Bagha N, Khavari R, Noroozpour H (2012) Seismic sources and neo-tectonics of Tehran Area (North Iran). Indian J Sci Technol 5:2379–2383

Badde DS, Gupta AK, Patki VK (2012) Cascade and feed forward back propagation artificial neural network models for prediction of compressive strength of ready mix concrete. In: Second International Conference on Emerging Trends in Engineering (SICETE), Dr. J.J. Magdum College of Engineering, Jaysingpur, India, vol.3, pp 1–6

Bartlett, P. (1997). Book review: Neural networks for pattern recognition. In: CM Bishop (ed.), Oxford University Press, New York, 1995. no. of pages: XVII+512. Statistics in Medicine, vol 16, pp 2385–2386

Bishop CM (1995) Neural Networks for Pattern Recognition. Oxford University Press

Breiman L (2001) Machine Learning. 45(1):5–32. https://doi.org/10.1023/a:1010933404324

Derafshi M, Kadkhodaie A, Rahimpour-Bonab H, Kadkhodaie R, Moslman-Nejad H, Ahmadi A (2022) Investigation and prediction of pore type system by integrating velocity deviation log, petrographic data and mercury injection capillary pressure curves in the Fahliyan Formation, the Persian Gulf Basin. Carbonates Evaporites 38:22

Dong S, Zeng L, Lyu W, Xu C, Liu J, Mao Z, Tian H, Sun F (2020) Fracture identification by semi-supervised learning using conventional logs in tight sandstones of Ordos Basin, China. J Nat Gas Sci Eng 76:103131. https://doi.org/10.1016/j.jngse.2019.103131

Ehsani J, Arian M (2015) Quantitative analysis of relative tectonic activity in the Jarahi-Hendijan Basin Area, Zagros Iran. Geosci J 19:1–15

Elbita A, Qahwaji R, Ipson S, Sharif MS, Ghanchi F (2014) Preparation of 2D sequences of corneal images for 3D model building. Comput Methods Programs Biomed 114(2):194–205. https://doi.org/10.1016/j.cmpb.2014.01.009

Ganesh SS, Arulmozhivarman P, Tatavarti VS (2018) Prediction of PM2.5 using an ensemble of artificial neural networks and regression models. J Ambient Intell Hum Comput. https://doi.org/10.1007/s12652-018-0801-8

Garson GD (1991) Interpreting neural-network connection weights. AI Expert 6(4):46–51

Gündoğdu S, Elbir T (2021) Application of feed forward and Cascade forward neural network models for prediction of hourly ambient air temperature based on MERRA-2 reanalysis data in a coastal area of Turkey. Meteorol Atmos Phys 133(5):1481–1493. https://doi.org/10.1007/s00703-021-00821-1

Hedayat A, Davilu H, Barfrosh AA, Sepanloo K (2009) Estimation of research reactor core parameters using cascade feed forward artificial neural networks. Prog Nucl Energy 51(6–7):709–718. https://doi.org/10.1016/j.pnucene.2009.03.004

Hosseinzadeh S, Kadkhodaie A, Wood D, Rezaee R, Kadkhodaie R (2023) Discrete fracture modeling by integrating image logs, seismic attributes, and production data: a case study from Ilam and Sarvak Formations, Danan Oilfield, southwest of Iran. J Petrol Explor Prod Technol 13:1053–1083

Huang G-B, Zhu Q-Y, Siew C-K (2006) Extreme learning machine: theory and applications. Neurocomputing 70(1–3):489–501. https://doi.org/10.1016/j.neucom.2005.12.126

Ja'fari A, Kadkhodaie-Ilkhchi A, Sharghi Y, Ghanavati K (2011) Fracture density estimation from petrophysical log data using the adaptive neuro-fuzzy inference system. J Geophys Eng 9(1):105–114. https://doi.org/10.1088/1742-2132/9/1/013

Kadkhodaie R, Kadkhodaie A, Rezaee R (2021) Study of pore system properties of tight gas sandstones based on analysis of the seismically derived velocity deviation log: a case study from the Perth Basin of western Australia. J Petrol Sci Eng 196:108077

Karaca Y (2016) Case study on artificial neural networks and applications. Appl Math Sci 10:2225–2237. https://doi.org/10.12988/ams.2016.65174

Khavari R, Arian M, Ghorashi M (2009) Neotectonics of the South Central Alborz Drainage Basin, in NW Tehran, N Iran. J Appl Sci 9:4115–4126

Kosari E, Ghareh-Cheloo S, Kadkhodaie-Ilkhchi A, Bahroudi A (2015) Fracture characterization by fusion of geophysical and geomechanical data: a case study from the Asmari reservoir, the Central Zagros fold-thrust belt. J Geophys Eng 12(1):130–143

Kosari E, Kadkhodaie A, Bahroudi A, Chehrazi A, Talebian M (2017) An integrated approach to study the impact of fractures distribution on the Ilam-Sarvak carbonate reservoirs: a case study from the Strait of Hormuz, the Persian Gulf. J Petrol Sci Eng 152:104–115

Lei C, Deng J, Cao K, Ma L, Xiao Y, Ren L (2018) A random forest approach for predicting coal spontaneous combustion. Fuel 223:63–73. https://doi.org/10.1016/j.fuel.2018.03.005

Mahmoodi K, Ghassemi H (2018) Outlier detection in Ocean Wave measurements by using unsupervised data mining methods. Polish Marit Res 25(1):44–50. https://doi.org/10.2478/pomr-2018-0005

Mansouri E, Feizi F, Jafari Rad A, Arian M (2017) A comparative analysis of index overlay and topsis (based on ahp weight) for Iron Skarn Mineral prospectivity mapping, a case study in Sarvian Area Markazi Province, Iran. Bull Miner Res Explor 155:147–160

Mansouri E, Feizi F, Jafari Rad A, Arian M (2018) Remote-sensing data processing with the multivariate regression analysis method for iron mineral resource potential mapping: a case study in the Sarvian area, central Iran. Solid Earth 9(2):373–384

Matin SS, Chelgani SC (2016) Estimation of coal gross calorific value based on various analyses by random forest method. Fuel 177:274–278. https://doi.org/10.1016/j.fuel.2016.03.031

Matin SS, Hower JC, Farahzadi L, Chelgani SC (2016) Explaining relationships among various coal analyses with coal grindability index by random forest. Int J Miner Process 155:140–146. https://doi.org/10.1016/j.minpro.2016.08.015

Mazdarani A, Kadkhodaie A, Wood D, Soluki Z (2023) Natural fractures characterization by integration of FMI logs, well logs and core data: a case study from the Sarvak Formation (Iran). J Petrol Explor Prod Technol. https://doi.org/10.1007/s13202-023-01611-8

Mohammadi M-R, Hemmati-Sarapardeh A, Schaffie M, Husein MM, Ranjbar M (2021) Application of cascade forward neural network and group method of data handling to modeling crude oil pyrolysis during thermal enhanced oil recovery. J Petrol Sci Eng 205:108836. https://doi.org/10.1016/j.petrol.2021.108836

Mohana RM, Reddy CK, Anisha PR, Murthy BVR (2021) Withdrawn: random forest algorithms for the classification of tree-based ensemble. Mater Today Proc. https://doi.org/10.1016/j.matpr.2021.01.788

Nabilou M, Arian M, Afzal P, Adib A, Kazemi A (2018) Determination of relationship between basement faults and alteration zones in Bafq-Esfordi region, central Iran. Epis J Int Geosci 41(3):143–159

Narad S, Chavan P (2016) Cascade forward back-propagation neural network-based group authentication using (N, N) secret sharing scheme. Proc Comput Sci 78:185–191. https://doi.org/10.1016/j.procs.2016.02.032

Nouri R, Arian M (2017) Multifractal modeling of the gold mineralization in the Takab area (NW Iran). Arab J Geosci 10(5):105

Nouri R, Jafari MR, Arian M, Feizi F, Afzal P (2013a) Correlation between Cu mineralization and major faults using multifractal modelling in the Tarom Area (NW Iran). Geol Carpath 64:409–416

Nouri R, Jafari MR, Arian M, Feizi F, Afzal P (2013b) Prospection for copper mineralization with contribution of remote sensing, geochemical and mineralographical data in Abhar 1: 100,000 sheet, NW Iran. Arch Min Sci 58:1071–1084

Patki Vinayak K, Shrihari S, Manu B (2013) Water quality prediction in distribution system using cascade feed forward neural network. Int J Adv Technol Civ Eng. https://doi.org/10.47893/ijatce.2013.1056

Pejic M, Kharrat R, Kadkhodaie A, Azizmohammadi S, Ott H (2022) Influence of fracture types on oil production in naturally fractured reservoirs. Nergies 15(19):7321

Raikar RV, Nagesh Kumar D, Dey S (2004) End depth computation in inverted semicircular channels using Anns. Flow Meas Instrum 15(5–6):285–293. https://doi.org/10.1016/j.flowmeasinst.2004.06.003

Razaghian G, Beitollahi A, Pourkermani M, Arian M (2018) Determining seismotectonic provinces based on seismicity coefficients in Iran. J Geodyn 119:29–46

Robert AMM, Letouzey J, Kavoosi MA, Sherkati S, Muller C, Verges J, Aghanabati A (2014) Structural evolution of the Kope dagh fold

and thrust belt (NE Iran) and interactions with the south Caspian Sea basin and Amu Darya basin. Mar Pet Geol 57:68–87

Taesiri V, Pourkermani M, Sorbi A, Almasian M, Arian M (2020) Morphotectonics of Alborz Province (Iran): a case study using GIS method. Geotectonics 54(5):691–704

Tokhmchi B, Memarian H, Rezaee MR (2010) Estimation of the fracture density in fractured zones using petrophysical logs. J Petrol Sci Eng 72(1–2):206–213. https://doi.org/10.1016/j.petrol.2010.03.018

Vaghefi M, Mahmoodi K, Setayeshi S, Akbari M (2020) Application of artificial neural networks to predict flow velocity in a 180° sharp bend with and without a spur dike. Soft Comput 24(12):8805–8821. https://doi.org/10.1007/s00500-019-04413-5

Warsito B, Santoso R, Suparti, Yasin H (2018) Cascade forward neural network for time series prediction. J Phys Conf Ser 1025:012097. https://doi.org/10.1088/1742-6596/1025/1/012097

Zazoun RS (2013) Fracture density estimation from core and conventional well logs data using artificial neural networks: the Cambro-Ordovician reservoir of Mesdar Oil Field, Algeria. J Afr Earth Sc 83:55–73. https://doi.org/10.1016/j.jafrearsci.2013.03.003

Zerrouki AA, Aïfa T, Baddari K (2014) Prediction of natural fracture porosity from well log data by means of fuzzy ranking and an artificial neural network in Hassi Messaoud Oil Field, Algeria. J Petrol Sci Eng 115:78–89. https://doi.org/10.1016/j.petrol.2014.01.011

Zhao Z, Qin J, He Z, Li H, Yang Y, Zhang R (2020) Combining forward with recurrent neural networks for hourly air quality prediction in northwest of China. Environ Sci Pollut Res 27(23):28931–28948. https://doi.org/10.1007/s11356-020-08948-1